

This is a repository copy of An open-source porous media modelling approach to investigate thermohydraulic features of compact printed circuit heat exchangers.

White Rose Research Online URL for this paper: <a href="https://eprints.whiterose.ac.uk/id/eprint/232783/">https://eprints.whiterose.ac.uk/id/eprint/232783/</a>

Version: Published Version

#### Article:

McDermott, M. orcid.org/0000-0002-5091-7170 and He, S. orcid.org/0000-0003-0326-2447 (2024) An open-source porous media modelling approach to investigate thermohydraulic features of compact printed circuit heat exchangers. Nuclear Engineering and Design, 421. 113084. ISSN: 0029-5493

https://doi.org/10.1016/j.nucengdes.2024.113084

## Reuse

This article is distributed under the terms of the Creative Commons Attribution (CC BY) licence. This licence allows you to distribute, remix, tweak, and build upon the work, even commercially, as long as you credit the authors for the original work. More information and the full terms of the licence here: https://creativecommons.org/licenses/

#### Takedown

If you consider content in White Rose Research Online to be in breach of UK law, please notify us by emailing eprints@whiterose.ac.uk including the URL of the record and the reason for the withdrawal request.





Contents lists available at ScienceDirect

## **Nuclear Engineering and Design**

journal homepage: www.elsevier.com/locate/nucengdes





# An open-source porous media modelling approach to investigate thermohydraulic features of compact printed circuit heat exchangers

M. McDermott\*, S. He

University of Sheffield, Department of Mechanical Engineering, Sir Frederick Mappin Building, Mappin Street, Sheffield, S1 3JD, United Kingdom

#### ARTICLE INFO

#### Keywords: Nuclear thermo-hydraulics OpenFOAM Printed circuit heat exchanger Open-source

#### ABSTRACT

An experimental air-foil printed circuit heat exchanger (PCHE) with CO2 as a working fluid is numerically modelled and developed within the OpenFOAM environment as a freely available package for more general PCHE designs. The conjugate heat transfer solver (chtMultiRegionFoam) is adapted to include both the hot and cold fluid streams of the PCHE, along with the solid recuperator body, within three uniquely specified overlapping mesh regions. The fluid stream momentum equation is adapted to incorporate porosity, with the additional streamwise air-foil drag (friction factor) accounted for by the Darcy-Forcheimer porous media model. A simple linear ad-hoc model for the transverse friction factor is evaluated to determine the dispersion of the momentum across the flow. Heat transfer between the fluid streams and the solid body is driven by a volumetric thermal resistance with a cell volume-weighted interpolation method (volume-to-volume coupling), with experimentally determined Nusselt number correlations applied. Temperature-dependent parameters based on isobaric NIST data for CO2 are tabulated as a user library and integrated within the coding package. The model predictions of the solid body temperature distributions are assessed and validated against experimental data with eight equidistant fibre optical measurements across the PCHE core and compared against finite-element-based MATLAB numerical results. Thermal stresses are evaluated and qualitatively evaluated against experimental data, demonstrating the capability of the model to highlight potential design features for improvement.

#### 1. Introduction

The development of next-generation nuclear reactors (Gen IV) has garnered significant interest over the past decade due to their improved efficiency, economics, and safety, which makes them promising lowcarbon emission solutions for future energy production. These reactors are specifically designed to withstand higher pressures and operating temperatures compared to previous plants (Xiuqing et al., 2006), with some designs such as liquid-metal fast reactors (LMFR) that use printed circuit heat exchangers (PCHE) to facilitate heat transfer from the nuclear reactor to the power cycle (Locatelli et al., 2013; Nestell and Sham, 2015). PCHEs typically consist of alternating stacked metal plates, with small working hot and cold fluid channels within each plate that are diffusion bonded together to form a solid block. These heat exchangers exhibit a high heat transfer area-to-flow volume ratio, achieved through chemically etched patterns that form various configurations, including cross-, counter-, or multifluid flow passes. Etched patterns encompass straight channels, zigzag channels, S-shaped fins, and offset air-foils (Liu et al., 2020). As a result of their compactness

and thermal efficiency, PCHEs are highly favoured for implementation in Gen IV nuclear power plants.

Detailed thermal hydraulic analysis is required to determine the performance of PCHEs and potential design flaws, which is necessary to certify a nuclear service PCHE design. Sophisticated analysis methods are required since stresses in PCHEs manifest themselves on the microchannel scale, while their driving loads must be resolved over the entire heat exchanger. As a result, traditional finite element (FE) and computational fluid dynamics (CFD) methods to model domain-scale thermal transients yield billion degree-of-freedom (DoF) problems that are slow to solve and cumbersome to adapt to varying PCHE designs. Thus, a simplified and flexible thermohydraulic modelling approach is needed. One approach is the effectiveness number of transfer units  $(\varepsilon - NTU)$  method, which is commonly used for the preliminary design and sizing of PCHEs. For example, Kim and No (2012) utilised the  $\varepsilon-NTU$  method along with CFD analysis to optimise the design and size of a PCHE used in a high-temperature gas reactor. The  $\varepsilon$  - NTUmethod provides a convenient approach to estimating the thermal performance of PCHEs in the early stages of design, where detailed

E-mail addresses: m.mcdermott@sheffield.ac.uk (M. McDermott), s.he@sheffield.ac.uk (S. He).

<sup>\*</sup> Corresponding author.

Thermal conductivity [W m <sup>-1</sup> K <sup>-1</sup> ]
Dynamic viscosity [Pa s]
Porosity [–]
Density [kg m <sup>-3</sup> ]
Surface area density [m <sup>-2</sup> ]
Cross-flow factor [–]
Specific heat capacity [J kg <sup>-1</sup> K <sup>-1</sup> ]
Hydraulic diameter [m]
Depth of the solid [m]
Friction factor [–]
Local heat transfer coefficient [W m <sup>-2</sup> K <sup>-1</sup> ]
Colburn factor [-]
Length of central channel [m]
Nusselt Number [–]
Dynamic pressure [Pa]
Hydrostatic pressure [Pa]
Prandtl number [–]
Volumetric thermal resistance [K m <sup>3</sup> W <sup>-1</sup> ]
Reynolds Number [–]
Temperature [K]
Velocity [m s <sup>-1</sup> ]
Volume [m <sup>3</sup> ]
Width of central channel [m]
Width of the solid [m]
Streamwise, transverse, and spanwise di-
rections [–]
Parallel
Perpendicular
Cold stream
Hot stream
Einstein tensor notation
Liquid stream (hot or cold)
Solid body

geometry information is not yet available. However, when it comes to detailed component-level analysis, more sophisticated models are required to accurately capture thermal performance and resolve thermal gradients within the PCHE. Variations in fluid properties, changes in channel geometry, and transitions between fluid inlets, outlets, and the counterflow core have a significant impact on thermal performance, which cannot be adequately captured by simple  $\varepsilon-NTU$  methods.

Linearised and homogenisation methods have been proposed to address these challenges. Both approaches use estimations for (a) the pressure drop from the fluid streams for a given mass flux and (b) the heat transfer to and from the PCHE solid body and fluid streams. The use of friction factor, f, is commonly used to express the pressure drop performance of a PCHE microchannel. Heat transfer effectiveness is described by the local heat transfer coefficient, h, or its dimensionless equivalents: Nusselt number, Nu and Colburn factor, j. All these terms can be determined through experiments, with microchannel CFD simulations or a combination of both Aneesh et al. (2016). Linearised analysis focuses on the PCHE core and transition regions.

It reduces the behaviour of these regions along the PCHE axis and employs one-dimensional discretisation and finite-difference methods to approximate the fluid-to-fluid heat transfer. Linearised models are effective in capturing the overall performance of the PCHE and can account for variations in fluid properties, such as near-critical operating conditions. They provide a valuable tool for preliminary design and system-level analysis.

For more detailed analyses, homogenisation methods are used to address all regions of the PCHE within a single 2D or 3D model. These methods homogenise the behaviour of microchannelled regions within representative volumes and formulate the thermohydraulic problem as a system of partial differential equations (PDEs). Urquiza et al. (2013) formulated an effective porous media model for a composite plate with offset fins for a liquid salt plate and helium plate. This composite plate was further divided into several zones containing unique geometrical configurations that include repetitive small-scale features. Unit cells containing these characteristics, which are also representative of the zones from which they were obtained, are then analysed and their effective thermal, hydraulic, and mechanical properties are derived. The model could capture the entrance, transition, core, exit, and solid PCHE regions. Using a porous media model for the hydraulic equations. the model captured the two-dimensional flow. Urquiza's work proved the applicability of the homogenisation method in the thermohydraulic modelling of PCHE but was limited in its implementation of finite differences and the assembly of boundary conditions in regions of nonlinearity proved to be unstable. Jentz (2021) applied the principles of Urquiza et al. (2013) for a finite element-based representation as a MATLAB package with a developed Heat Exchanger Thermohydraulic (HHXT) environment for both an air-foil and a zigzag channel recuperator. The HHXT provides a multistream heat transfer solution in 2D or 3D for full-sized heat exchangers without needing to resolve the specific microchannel geometries. This is achieved through a finite element solution of a system of coupled nonlinear PDEs which model the following behaviour: core solid thermal conduction, nonlinear porous media flow in each fluid stream, thermal advection in each fluid stream, heat transfer between each fluid stream and the core solid, and thermal storage in the core and all fluids. The results of the modelling predict the recuperator temperature well against the experimental data, with further analysis of the thermal and mechanical stress gradients on the system (Jentz, 2021).

There have been many attempts to capture thermohydraulic features of both the domain scale and pore scale of heat exchangers with CFD-based approaches. Many of the pore-scale approaches utilise the full Navier-Stokes equations and accompanying energy equation over a representative unit cell with an eddy-viscosity RANS model for the working fluids. Cong et al. (2021) applied a SST  $k - \omega$  and Abid low Reynolds  $k - \varepsilon$  turbulence model for sCO2 and liquid sodium, respectively, with a segregated coupling strategy for conjugate heat transfer. A four-equation model was proposed for the same working fluids (Su et al., 2023; Li et al., 2022), which assesses the variability of the Prandtl number due to the normal Reynolds analogy for the breakdown of the heat flux for the liquid sodium. Hakim et al. assessed the thermohydraulic performance of cube fin structures in a PCHE (El-Hakim et al., 2022) with also an SST  $k - \omega$  model. In other works, a C-shaped channel geometry has been optimised utilising 3D RANS and machine learning techniques to improve the overall performance of the C-shaped PCHE (Saeed et al., 2022). In terms of a multiscale approach, Greiciunas et al. (2019) modelled a plate fin HX by taking a section of a HX core and modelling both cold and hot streams separated by a conducting solid, implemented using a conjugate heat transfer methodology. The HX section domain data were implemented in the macro HX unit models, where the HX core was simplified using porous media and effectiveness models for flow and heat transfer. Della Torre et al. (2019) proposed a similar approach for a multiscale model to predict the various scales of an offset-strip fin and dimple-type turbulator for the automotive industry.

Developing user-friendly and adaptable coding packages is advantageous for the advancement of nuclear energy systems. Some of the mentioned works are developed with in-house codes (Jentz, 2021; Urquiza et al., 2013), commercial codes (Dmitriev et al., 2023), or open source codes that are not available, such as OpenFOAM (Greiciunas et al., 2019; Su et al., 2023; Della Torre et al., 2019). The study of various systems with a porous media methodology with OpenFOAM coding packages has attracted much interest. Higuera et al. (2014) and Feichtner et al. (2021) created IHFOAM by adapting pre-existing code to study flow through coastal structures. He et al. (2022) developed PorousDriftFoam to model shell and tube heat exchangers. Maes and Menke (2022) created GeoChemFoam to solve complex flow processes including multiphase transport with interface transfer, single phase flow in multiscale porous media, and reactive transport with mineral dissolution. Zuk et al. (2022) presented porousGasificationFoam for comprehensive simulations of thermochemical conversion in porous media. The code development in this work is partly inspired by the application of these OpenFOAM packages, which are available on GitHub (https://github.com/MikeMcDermott-Code/PCHE).

This work aims to develop a methodology to analyse the macroscale thermohydraulic characteristics of PCHEs in the finite-volume Open-FOAM environment as an open-source package. The methodology differs from the finite element approach of Jentz and Anderson (2020) by considering three separate unique regions (hot stream, cold stream, and solid body) and by solving the hydraulic solution with the full Navier-Stokes equation with the same friction factor imposed as the experimental correlations. The assumption of cross-flow variations is examined, and the hydraulic solution is calculated. Convective heat transfer is addressed with a volume resistance between fluid streams and the solid body  $R_{s\rightarrow l}$ , with a cellVolumeWeight interpolation method (volume-tovolume coupling) using the OpenFOAM functionality. The experimental air-foil PCHE is used as an example case to validate the current method against previous simulation results and experimental data. The current work forms the basis of the macro-scale approach, and an accompanying coupled multiscale approach is ongoing. The paper is organised as follows: Section 2 presents the methodology & governing equations; Section 3 presents the numerical procedure and OpenFOAM code package; Section 4 presents the results with an example case for the air-foil PCHE with thermal-hydraulic predictions and analysis of fluid streams and temperature of the recuperator body; and finally, Section 5 draws conclusions.

#### 2. Methodology & Governing equations

The finite volume (FV) approach is employed to evaluate the macroscopic PCHE thermohydraulic features with a 2D homogenised porous media representation. Fig. 1 shows a schematic of the methodology for this study. The entire PCHE is represented by stacked alternating plates in which the modeller identifies the number of unique plates (e.g. hot stream h, and cold stream c). On the pore-scale, the internal flow follows tortuous paths for a given etching, such as open and closed channels. In the porous-media approach, the PCHE is represented by its volume-averaged properties via a geometrically defined porous region of volumetric dimension. In this continuous and homogeneous porous region, resistance source terms are applied as closure terms to the momentum equation. The source terms represent the macroscopic effects of the porous structure on the flow. The modeller must identify, through experiment or analytical calculations, the surface area density  $A_{\rm surf}$  and the hydraulic diameter,  $D_h$ , of the unique fluid streams. In PCHEs, the thermohydraulic flow is dominated by streamwise (x) and transverse (y) motion, and thus spanwise (z) motion variation can be assumed negligible and reduce the problem to 2D. The domain is divided into regions: one solid body and l unique fluid streams. Although in Fig. 1 the regions are separated for visual aid, they exist in the same x-y plane, with a fixed thickness to ensure volume fluxes (however still 2D in nature). The volume of all the homogenised regions is specified

by V, with the porosity of the fluid regions determined experimentally via the relationship  $\phi_l = V_l/V$ . The porosity becomes essential for identifying the volumetric heat transfer to and from the fluid streams and solid body, as well as the additional frictional losses, f, both parallel  $f_{\parallel}$ , and perpendicular  $f_{\perp}$ , within the fluid streams. The volume averaged thermal and hydraulic transport equations for the solid body and fluid streams are described below. In what follows, conventional tensor notation is applied with subscript i and j denoting indexes, and kk denoting the trace. Subscript l and s represent properties of the fluid stream and solid body, respectively, with all other subscripts clarified when necessary.

#### 2.1. Transport equation for the solid body

The volume-averaged specific enthalpy transport equation for the solid body is given by,

$$\frac{\partial \rho_s c_p \langle T_s \rangle}{\partial t} = \frac{\partial}{\partial x_j} \left( \kappa_s \frac{\partial \langle T_s \rangle}{\partial x_j} \right) + \sum_{l=1}^L \left( \frac{\langle T_s \rangle - \langle T_l \rangle}{R_{s \to l}} \right), \tag{1}$$

where  $\rho_s$  is the solid density,  $\kappa_s$  is the solid thermal conductivity coefficient,  $T_s$  is the solid temperature, and  $T_l$  is the fluid stream temperature. The symbol  $\langle \cdot \rangle$  stands for the local phase average (integral over the entire control volume). For brevity, the relationship between the local phase average and local phase intrinsic average (integral over the fraction of the control volume occupied by the solid) is given by  $\langle \cdot \rangle = \phi_s \langle \cdot \rangle^s$ . Similarly is the case for the fluid such that  $\langle \cdot \rangle = \phi_l \langle \cdot \rangle^l$ . The term on the LHS of Eq. (1) represents the total heat storage within the homogenised volume. Although this term becomes negligible for steady state, it has some pseudotransience effects during start-up, which can impact thermal gradients and stress. The first term on the RHS of Eq. (1) represents solid conduction. The last term represents the total heat exchange to L fluid streams, with solid-to-fluid heat transfer driven by volumetric thermal resistance,  $R_{s\rightarrow l}$ . This parameter can be either a constant or derived from a heat transfer coefficient. The dimensional fluid heat transfer coefficient,  $h_l$ , is the easiest to use and allows  $R_{s\rightarrow l}$ to be written in terms of the internal microchannel hydraulic diameter,

$$R_{s \to l} = \frac{1}{h_l} \times \frac{V}{A_{\text{surf},l}} \equiv \frac{1}{4} \left( \frac{D_h}{\phi h} \right)_l. \tag{2}$$

For PCHE flow problems,  $h_l$  depends on fluid properties such as local velocity variation, porosity, and Nusselt number, determined through experimental correlation, which is specified further in this study in the fluid stream transport equations. In the case of a two-stream problem (hot and cold), the last term in Eq. (1) is simplified by

$$\sum_{l=1}^{L} \left( \frac{\langle T_s \rangle - \langle T_l \rangle}{R_{s \to l}} \right) = \frac{\langle T_s \rangle - \langle T_c \rangle}{R_{s \to c}} + \frac{\langle T_s \rangle - \langle T_h \rangle}{R_{s \to h}}.$$
 (3)

### 2.2. Transport equations for l fluid streams

The volume-averaged transport equations for the mass and momentum of the fluid streams are given respectively by

$$\frac{\partial \rho_l \langle U_{i,l} \rangle}{\partial x_i} = 0,\tag{4}$$

$$\frac{\partial \rho_l \langle U_{i,l} \rangle}{\partial t} + \langle U_{j,l} \rangle \frac{\partial \rho_l \langle U_{i,l} \rangle}{\partial x_j} = -\frac{\partial \langle P_l \rangle}{\partial x_i} + \frac{\partial}{\partial x_j} \left( \mu_l \frac{\partial \langle U_{i,l} \rangle}{\partial x_j} \right) + S_i, \tag{5}$$

where  $\langle U_{i,l} \rangle$  is known as the superficial fluid velocity (or Darcy velocity),  $\rho_{i,l}$  is the fluid density,  $P_l$  is the dynamic pressure, and  $\mu_l$  is the dynamic viscosity. The additional pressure resistance from the internal micro-channels is represented as a momentum source term given by the Darcy–Forchheimer model (Whitaker, 1996),

$$S_{i} = -\left(\frac{\rho f_{i}}{2D_{h}} \left| \frac{\langle U \rangle}{\phi} \right| \right)_{l} \frac{\langle U_{i,l} \rangle}{\phi_{l}},\tag{6}$$

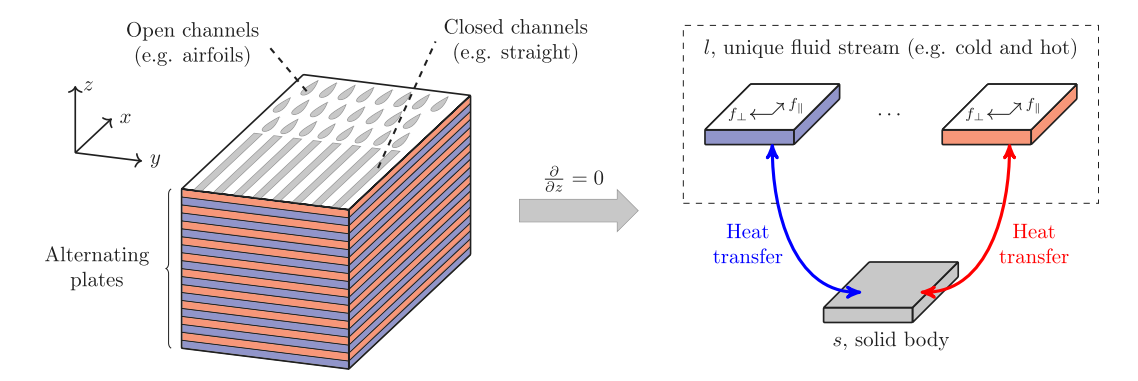


Fig. 1. Schematic of the general methodology for homogenised PCHE.

where  $|U_l|$  is the superficial fluid velocity magnitude. The Forchheimer coefficient (or friction factor term) is given by  $f_i$ , which is typically calculated using correlations from experimental data or purposefully built CFD studies, with functional form based on the Reynolds number, viz.

$$\frac{1}{\sqrt{f(Re)}} = A \log_{10} \left( B + \frac{C}{Re\sqrt{f(Re)}} \right), \tag{7}$$

where A, B, and C are determined constants. The Reynolds number is defined by the following:

$$Re_{l} = \frac{\rho_{l} |\langle U_{l} \rangle| D_{h,l}}{\phi_{l} \mu_{l}}, \tag{8}$$

which is computed by the modeller within a specified range. Other functional forms of Eq. (7) exist within the literature (Liu et al., 2020) depending on the nature of the fluid (e.g. sodium, carbon dioxide, helium) and the canonical system examined (e.g. channel etchings), although not discussed further in this study.

The modeller must consider the directionality of  $f_i$  within the specified homogenised volume, which follows the flow channels or mean flow direction by  $f_{\parallel}=f(Re)$ , and the transverse (cross-flow) component by  $f_{\perp}$  (see Fig. 1). Here a simple linear ad hoc model is prescribed for the cross-flow component such that  $f_{\perp}=C_ff_{\parallel}$ , where  $C_f>1$  is the cross-flow factor. Within PCHEs, for both open and closed channels, there exists strong resistance to transverse momentum maldistribution (although not infinite) as a result of the fine detailed internal micro-channel structures. A porous media (PM) study on shell and tube heat exchangers (STHE) examined the value of  $C_f$  (named the resistance factor in their study), predicting the pressure gradient within 10% error compared to fully resolved CFD simulations, when  $C_f>100$ . They concluded that the PM approach is a powerful tool for modelling PCHE hydrodynamics (Zhu et al., 2022). The validity of the cross-flow application in the context of PCHEs is examined further in this paper.

The corresponding volume-averaged fluid-specific enthalpy transport equation is given by,

$$\frac{\partial \rho_l c_p \langle T_l \rangle}{\partial t} + \langle U_{j,l} \rangle \frac{\partial \rho_l c_p \langle T_l \rangle}{\partial x_j} = \frac{\partial}{\partial x_j} \left( \kappa_l \frac{\partial \langle T_l \rangle}{\partial x_j} \right) - \frac{\langle T_s \rangle - \langle T_l \rangle}{R_{s \to l}}, \tag{9}$$

where  $c_{p,l}$  is the fluid specific heat capacity, and  $\kappa_l$  is the fluid thermal conductivity. Similarly to the enthalpy transport of the solid body (Eq. (1)), the first term on the LHS of Eq. (9) determines fluid heat storage and the second term additionally drives fluid heat advection (not present in Eq. (1) because  $U_{j,s}$  is zero). The first term on the RHS is fluid conduction, and the second term accounts for fluid-to-solid heat transfer, noting the opposite sign which balances the overall total heat transfer. The volumetric thermal resistance between the solid and the fluid streams, defined generally earlier (Eq. (2)), is presented here as a function of the Nusselt number such that,

$$R_{s\to l} = \frac{1}{4} \left( \frac{D_h^2}{\phi \kappa N u} \right)_l,\tag{10}$$

with functional form

$$Nu_l = aRe_l^b Pr_l^c, (11)$$

where a, b and c are determined constants, and the Reynolds number and Prandtl number are specified within a range. As with the friction factor correlation (Eq. (7)), the Nusselt number correlation (Eq. (11)) can take various forms, such as the dependence on the Peclet number ( $Pe = ReP_{t_t}$ ) for low-Prandtl fluids such as sodium hot liquid.

#### 3. Numerical procedure & OpenFOAM

A numerical framework is built using OpenFOAM (v2212) based on the methodology and governing equations described in the previous section. The tree structure of the coding package is described in Fig. 2, showing three main branches: the solver (mySolvers/PCHEFoam), case directory (run/PCHE), and library (myLibs/PoroVHT). The inbuilt chtMultiRegionSimpleFoam solver is used and adapted to incorporate the governing equations, named PCHEFoam. This includes the addition of fluid porosity (named PoroFluid) as a volScalarField within createFluidFields.H and UEqn.H. The momentum and energy source terms are solved using the inbuilt interRegion finite volume option (fvOptions), with the sub-classes explicitPorositySource and variableHeatTransfer, respectively, with the latter being adapted to incorporate the fluid porosity (named PoroVHT).

The case directory (run/PCHE) contains the usual structure for standard OpenFOAM simulations, with a 0 time directory, system directory, and constant directory. First, the modeller must identify the unique regions of the PCHE design, which are specified within regionProperties. Here, the fluid streams have been represented as 1-stream which, for brevity, are HotStream and ColdStream for our purpose. The geometry of the fluid flows and the solid body is generated within blockMeshDict. The setFieldsDict functionality allows the user to specify spatially varying fluid porosity,  $\phi_l(x_i)$ , for cases where there are known differences in microchannel density. Cell zones that specify the directionality of the friction factor within the fluid regions are assigned within topoSetDict, or directly via the blockMeshDict functionality. The local coordinate system for each cell zone specified is defined within fvOptions for the fluid streams, which is dynamically linked to the root Open-FOAM directory etc/caseDicts. Also applied within fvOptions is the limitTemperature functionality for all regions, which bounds the temperature field between the hot inlet and cold inlet temperatures and enhances numerical stability during run time.

The temperature-dependent fluid properties are defined within thermophysicalProperties using the tabulated OpenFOAM functionality. These tabulated values are predetermined based on isobaric data collected from the NIST database and stored and dynamically linked in the thermoData library within the case directory. The example shown in Fig. 2 is for CO<sub>2</sub>, with the file p<value> representing

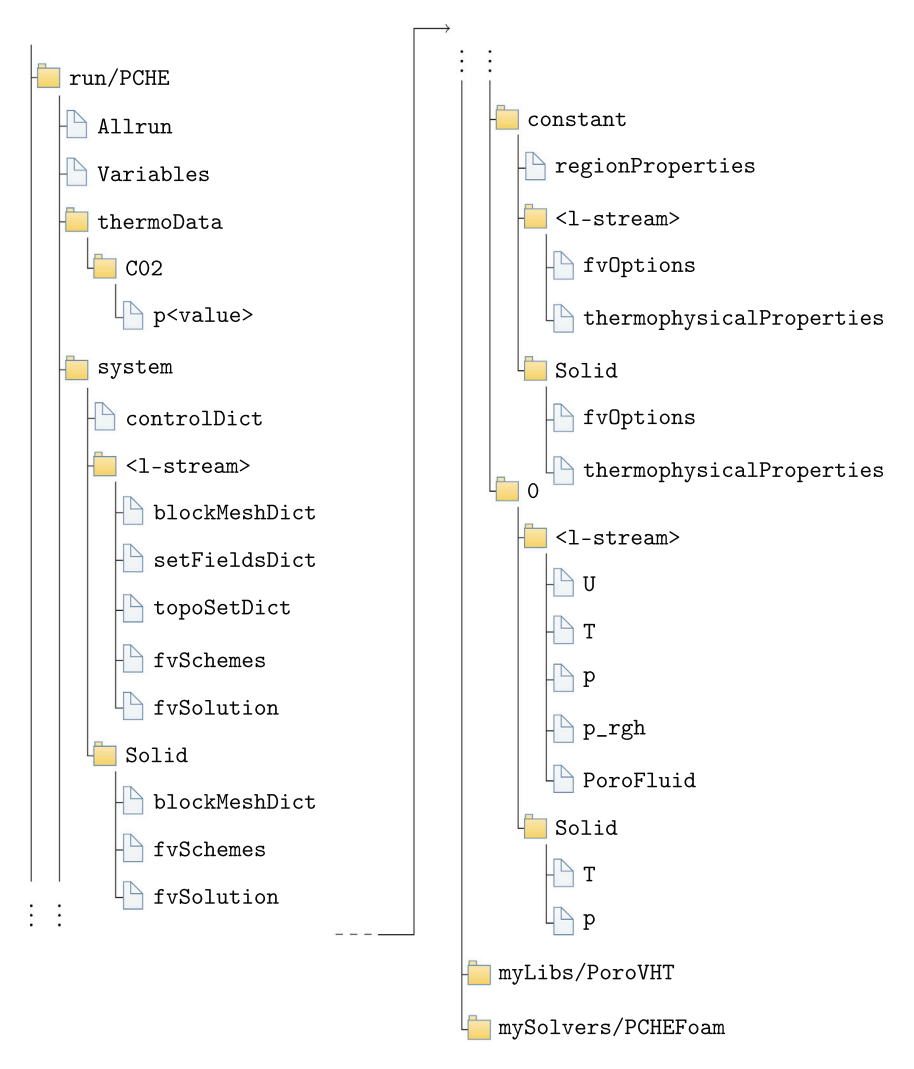


Fig. 2. OpenFOAM code tree structure for PCHE simulations.

the isobaric data at a given pressure constant (e.g. p5,990 could be a pressure of 5.990 [MPa]). A more expansive library could be included for  $\rm CO_2$  over temperature and pressure, or for varying fluids such as helium and liquid sodium, but it is beyond the scope of this work.

The initial values of the fluid and the boundary conditions are stored in the 0 time directory. A constant mass flow rate condition is imposed on the inlet and outlet of the velocity field with the flowRateInletVelocity boundary condition. The temperature field has a Dirchelet conditions (fixedValue) at the inlet and Neumann conditions (zeroGradient) at the outlet. The hydrostatic pressure  $(P_{rgh})$  uses a fixed flux condition at the inlet with fixedFluxPressure and a fixedValue condition at the outlet, with also 0 gauge pressure for both  $P_{rgh}$  and P. With this approach, the dynamic pressure, P, is set to calculated on all boundaries. At walls, the velocity field has a slip condition due to the boundary layer not being fully resolved based on the porous media approach, with all other fields having zeroGradient. The boundary conditions for the solid are simply zeroGradient everywhere for the temperature. The solid pressure field is included within the case as a place holder for the OpenFOAM structure and is set to 0 as with the gauge pressure. A summary of the boundary conditions for the fluid streams can be viewed in Table 1.

Gauss linear and upwind schemes are used for divergence and Laplacian terms within fvSchemes, and a PISO loop is used within fvSolution. All the adjustable variables (e.g. inlet temperature, mass flow rate, Nusselt number constants, friction factor constant, etc.) are written in a configuration file (Variables) in the main case directory

for easy adjustability. An Allrun script is also included within the main case directory, which cleans the case, runs the blockMesh application, sets the cell zones, and then runs the simulation with the PCHEFoam solver until a steady state is reached. The simulations were run on an ASUS ZenBook UX430U laptop with an Intel Core i7 processor and 8 GB of RAM, which took roughly 30 clock time seconds to complete.

#### 4. Example case: Airfoil CO<sub>2</sub>-CO<sub>2</sub> PCHE

The following section aims to use the current mathematical model and coding package with an example case for an airfoil PCHE with  $\rm CO_2$  as working fluids. Experimental investigations have been conducted on this airfoil PCHE, along with accompanying finite element-based analysis in Matlab (Jentz, 2021), both of which are used to validate the current modelling package by comparing against thermal data and simulation results.

#### 4.1. Computational domain

The airfoil PCHE consists of 5 cold  $\rm CO_2$ , 4 hot  $\rm CO_2$ , and 1 instrumented 1.5 [mm] thick plate. The hot and cold  $\rm CO_2$  plates contain a 1 [mm] deep etched, 94.3 [mm] wide, airfoil channel, containing 8.1 [mm] long NACA0020 airfoils spaced at 3.65 [mm] intervals across the flow and 6.9 [mm] along the flow direction (see Fig. 1 for airfoil visual). The hydraulic diameter is calculated as  $D_h = 1.498$  [mm]. The porosity of the core is calculated as  $\phi_{\rm core} = 0.4752$ , such that the

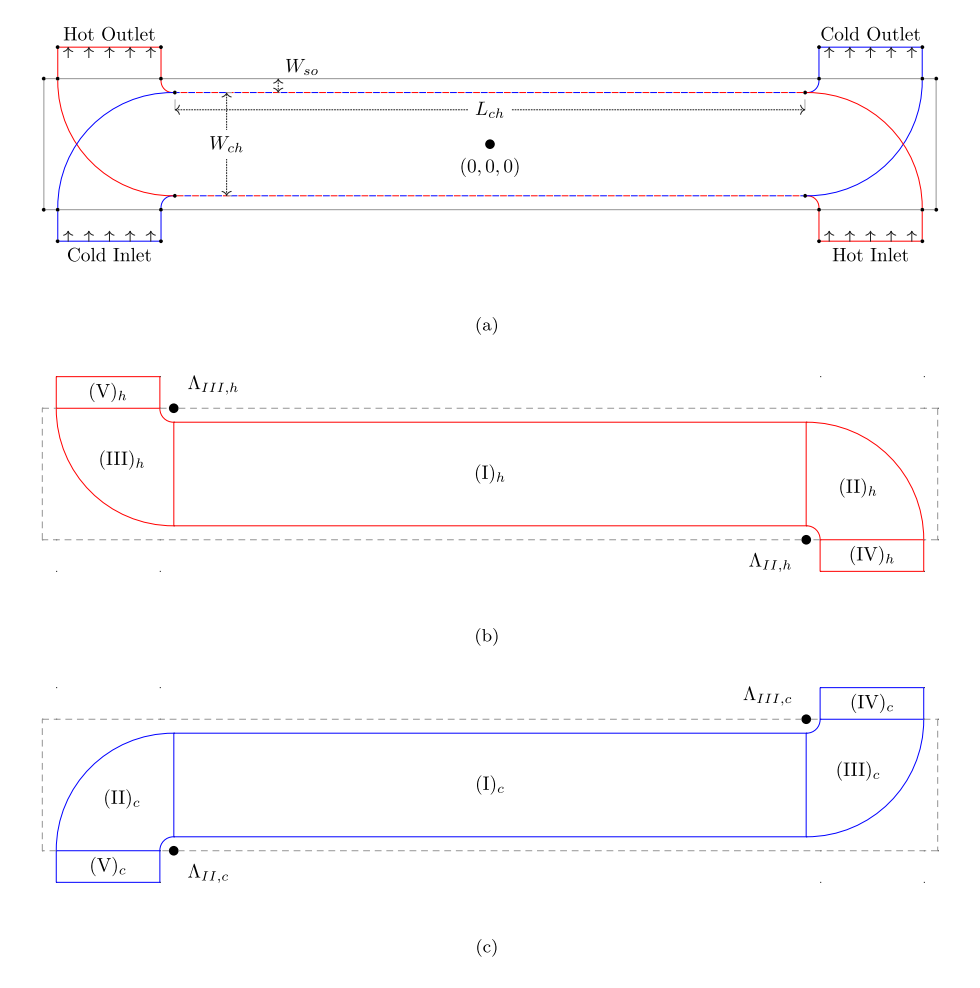


Fig. 3. (a) Computational domain of the solid body, hot stream and cold stream. Region cell zones for (b) hot stream, and (c) cold stream.

Table 1
Summary of model boundary conditions implemented in OpenFOAM for the fluid streams.

	Fluid boundary patch			
	Wall(s)	Inlet(s)	Outlet(s)	
$P_{rgh} \ T \ U$	fixedFluxPressure zeroGradient slip	fixedFluxPressure fixedValue flowRateInletVelocity	fixedValue zeroGradient inletOutlet	

porosities of the hot and cold fluid stream are  $\phi_c = \frac{5}{9}\phi_{\rm core} \approx 0.264$  and  $\phi_h = \frac{4}{9}\phi_{\rm core} \approx 0.211$ .

The computational domain for this study is constructed and shown in Fig. 3a. The solid body, hot stream, and cold stream regions are specified within the grey, red, and blue bounds, respectively. The dashed red-blue line represents both the hot- and cold-stream bounding lines. Each region exists within the same x-y plane, and although the model is 2D in nature, there is a finite depth of the solid body,  $D_{so}$ , which ensures the application of volume fluxes. The main dimensions labelled within Fig. 3a are specified as follows: length of the central channel,  $L_{ch} = 575.5$  [mm]; width of the central channel,  $W_{ch} = 94.3$  [mm]; width of the solid wall,  $W_{so} = 12.7$  [mm]; depth of the channel,  $D_{so} = 15$  [mm]. Fig. 3b & c displays the 5 cell zones for the hot and cold stream, namely: central channel (I), inlet curve (II), outlet curve (III), outlet (IV) and inlet (V). There are four coordinates,  $\Lambda$ , which denote the central point of rotation for a cylindrical coordinate transformation for the curved regions II and III (e.g.  $\Lambda_{II,h} = (\frac{1}{2}L_{ch}, -\frac{1}{2}W_{ch} - W_{so})$ ). This ensures that the imposed streamwise friction factor acts parallel to the channel and the analogous transverse term acts perpendicularly. The four geometric parameters and specifications of unique cell zones are purposefully defined, and the procedure that is presented can be extended to other PCHE designs (e.g varying inlet/out locations and multistream flow passes). A mesh independence study is conducted over 5 meshes by comparing outlet temperatures and pressure drop measurements, which can be viewed in Table 2. The M1 mesh gave rise to enthalpy residuals of  $10^{-2}$ , leading to spurious results. The M2 to M4 meshes gave convergent results, with no notable differences in the measurements for the M5 mesh. The M4 mesh is selected for this study, with a relatively fast CPU time of  $\sim 30$  [s].

#### 4.2. Model inputs & Properties

The model inputs and properties of the model are built within a single configuration file within the main directory of the OpenFOAM case file, as explained in Section 3 and Fig. 2. This encompasses the four geometry dimensions from the previous subsection; the friction factor and Nusselt number experimental values (from Eqs. (7) and (11)) within the fvOptions directories; initial and boundary conditions for temperature, pressure and mass flow rate for the hot and cold streams — all of which are summarised within Table 3, with boundary

**Table 2** Mesh independence analysis:  $x_{so}$  and  $y_{so}$  are the number of cells in the x and y direction for the solid, respectively. The total cells includes the solid and the two fluid meshes. Measured values are the outlet temperature, pressure drop and elapsed CPU time for each run.

Mesh	$x_{so}$	$y_{so}$	Total cells	T <sub>h,out</sub> [K]	$T_{c,out}$ [K]	$\Delta P_h$ [Pa]	$\Delta P_c$ [Pa]	CPU time [s]
M1	50	20	5800	319.28	419.78	8512	3927	10.84
M2	100	20	8800	318.50	420.49	7842	3203	13.85
М3	150	30	18900	318.33	420.73	7840	3200	28.43
M4	200	30	23 400	318.22	420.84	7839	3199	33.55
M5	400	50	73 000	318.22	420.83	7839	3199	110.56

Table 3
Summary of model inputs and parameter values for the airfoil PCHE.

	Units		Region		
		Cold	Hot	Solid	
fvOptions constants:					
Streamwise friction factor, $f_{\parallel}$	-	0.068	0.067	_	
Cross-flow friction factor, $f_{\perp}$	_	$1000f_{  }$	$1000f_{  }$	-	
Nusselt constant, a	_	0.023	0.023	-	
Reynolds power, b	_	0.8	0.8	-	
Prandtl number, Pr	_	0.85	0.85	-	
Prandtl number power, c	-	0.3	0.4	-	
Initial & Boundary conditions:					
Inlet temperature, $T_{\text{inlet}}$	K	296.65	475.45	_	
Mass flow rate, m	$kg \ s^{-1}$	0.05378	0.05378	-	
Parameters:					
Fluid pressure, $P_{ref}$	MPa	5.990	4.892	_	
Density, $\rho(T)$	$kg m^{-3}$			8030	
Specific heat capacity, $c_p(T)$	J kg <sup>-1</sup> K <sup>-1</sup>			533	
Viscosity, $\mu(T)$	Pas	Isobaric data		_	
Thermal conductivity, $\kappa(T)$	$W\ m^{-1}\ K^{-1}$			17.6	

 Table 4

 Comparison of model predictions of pressure drop and outlet temperature with experiment and Matlab FE results.

	Units	Case		
		Experiment	Matlab FE	Current model
$\Delta P_h$	Pa	$7250 \pm 230$	8150	7839
$\Delta P_c$		$4090 \pm 920$	3000	3199
$T_{h,outlet}$	K	$312.2 \pm 0.29$	313.73	318.22
$T_{c,outlet}$		$417.11 \pm 0.95$	421.07	420.84

conditions applied based on Table 1. The values of the friction factor constants of Eq. (7) are A=-2.0, B=0.08068, and C=43.1 from experimental measurement (Jentz, 2021), which determine the value of  $f_{\parallel}$  given the Reynolds number of  $Re_h=13780$  and  $Re_c=11340$  for the hot and cold stream, respectively.

The key thermal properties of the model are imported in the thermophysical Properties class with a dynamic library within OpenFOAM as described in Section 3. The solid body is 316 steel and has properties which are given constants. Fig. 4 displays the temperature-dependent  $\rm CO_2$  properties (symbols) at pressures  $P_c=4.892$  [MPa] (red) and  $P_h=5.990$  [MPa] (blue) for the hot and cold stream, respectively. The values were chosen to demonstrate the model's capability to capture thermohydraulic features close to the pseudo point (Jentz, 2021).

#### 4.3. Steady-state solution

Following the numerical procedure and simulation setup presented in the previous sections, the case file is run under a PISO algorithm until a steady-state solution ( $10^{-5}$  residuals). The results are gathered and presented below and discussed for the mean velocity and pressure, and the temperature distributions.

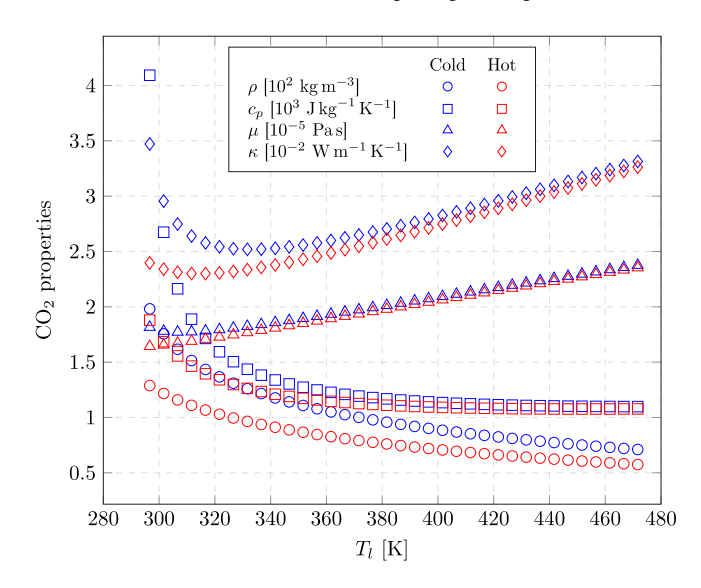


Fig. 4.  ${\rm CO_2}$  properties along isobars  $P_c=5.990$  [MPa] (blue) and  $P_h=4.892$  [MPa] (red) in the temperature range  $T_{\rm c,inlet}=296.65$  [K] to  $T_{\rm h,inlet}=475.45$  [K].

#### 4.3.1. Mean velocity and pressure

First, the cross-flow factor,  $C_f$ , presented in previous sections (governed by  $f_{\perp} = C_f f_{\parallel}$ ) is examined to determine the effect on the mean velocity. Fig. 5 displays the magnitude of the mean velocity of the hot stream with increasing variation of  $C_f$ . Fig. 5a represents the case with no airfoils, or no drag force present with  $f_{\parallel}=0$  and  $C_f = 0$ . The fluid enters the inlet with a mean distribution of  $U_{h,inlet} \approx$ 0.67 [m s<sup>-1</sup>]. As the fluid flow turns in the inlet curve and enters the central region, strong flow separation is observed, accompanied by large mean velocity differences. For the second case in Fig. 5b, with the presence of the streamwise drag force, and small cross flow factor, the transverse velocity dispersion is suppressed, although some effects remain due to the presence of strong radial pressure gradients created by the centrifugal force acting on the fluid in the bends. Between the third and fourth cases in Fig. 5c & d respectively, the velocity differences are minimised, which is what one would expect with a densely packed airfoil filled channel. Fig. 6 displays the transverse plots of the mean velocity with varying cross-flow factors,  $C_f = 1,10$ and 1000, measured at two streamwise locations:  $x = \frac{1}{4}L_{ch}$  (central channel) and  $x = \frac{1}{2}L_{ch}$  (inlet bend). The suppression of the transverse velocity distribution can be seen here for increasing cross-flow factor. The values of around  $C_f > 100$  for the STHE's case (Zhu et al., 2022) are recommended and is also the case for the current study on PCHE's, in which we use  $C_f = 1000$ .

Fig. 7 shows the contour plots of the mean fluid pressure of the hot and cold stream, with the velocity vectors superimposed. For the hot stream, there is an observed flow acceleration from the inlet to the outlet, and conversely with the cold stream, there is a flow deceleration. This is a result of the varying temperature-dependent parameters close to the pseudo point (such as viscosity and density) along with the fixed mass-flow condition. In both hot and cold streams, there is an almost linear pressure drop from the inlet to the outlet, resulting from the imposed resistance term of the momentum source with a high crossflow factor ( $C_f = 1000$ ). Experimentally, only the inlet and outlet conditions are well known, as it is challenging to obtain complete velocity and pressure data statistics within the PCHE flow channels. Table 4 displays the measured pressure drop for the current model and is cross-compared with the experimental data and the Matlab FE results. The current model predictions show a slight improvement compared with the Matlab results, and fall within the error bars of the experimental findings. It must be noted that pressure drop measurement

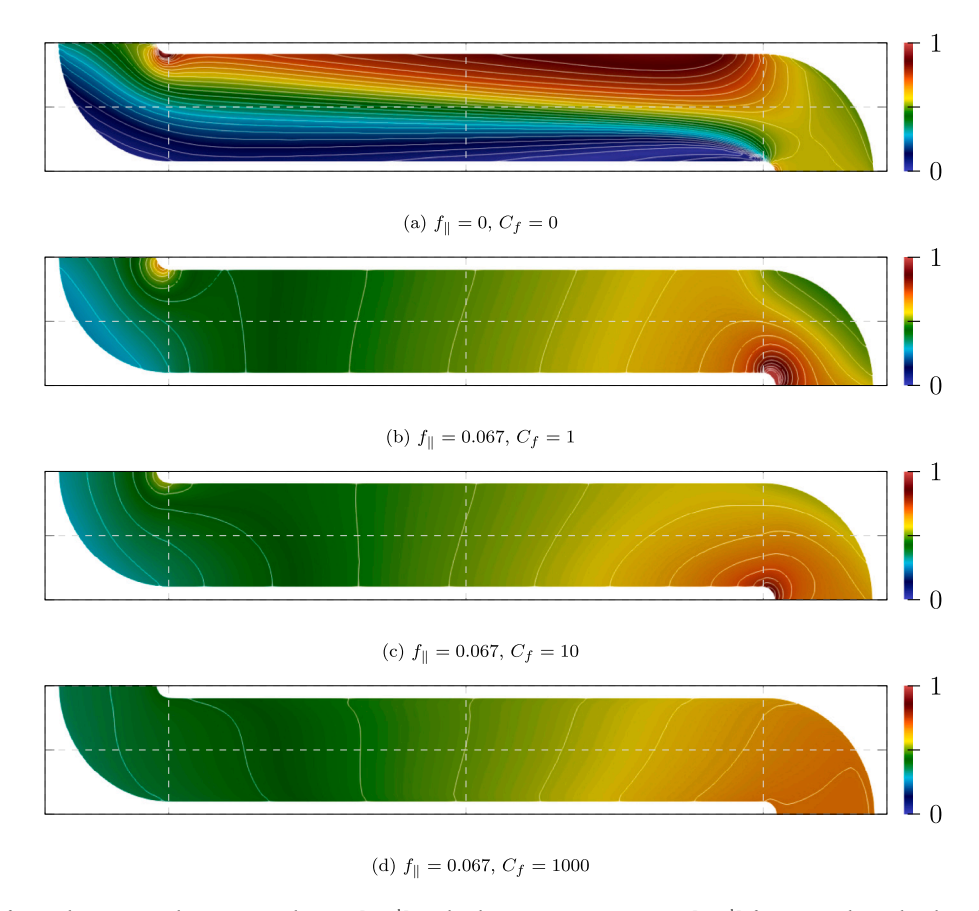


Fig. 5. Contour profiles of mean hot stream velocity magnitude,  $|U_h|$  [m s<sup>-1</sup>], with white contour spacing 1/25 [m s<sup>-1</sup>] for improved visuals. The colour ranges from 0 [m s<sup>-1</sup>] (blue) to 1 [m s<sup>-1</sup>] (red) for all panels. The panels from top to bottom show increasing cross-flow factor.

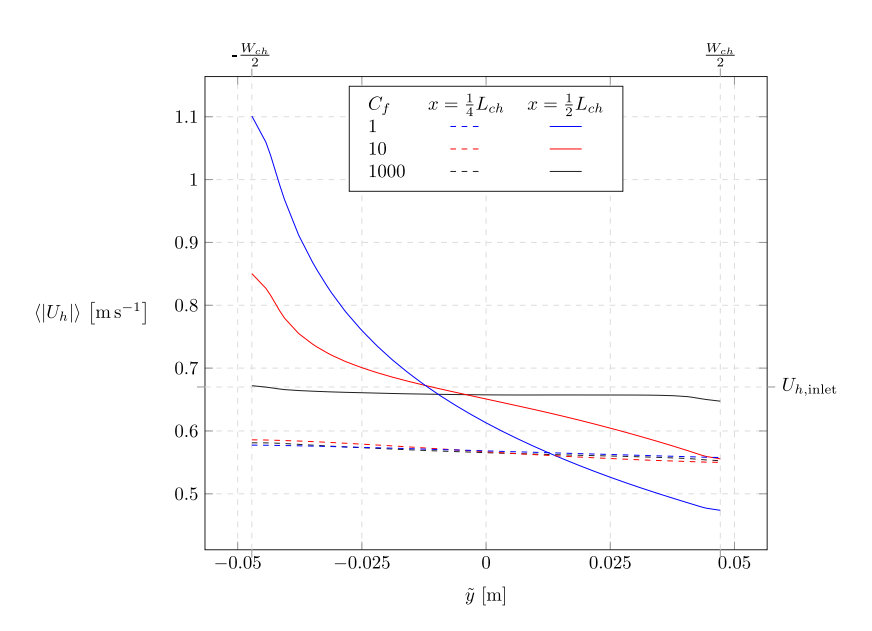


Fig. 6. Transverse plots of the mean hot stream velocity magnitude,  $|U_h|$  [m s<sup>-1</sup>], with varying cross-flow factor,  $C_f$ , measured at two streamwise locations:  $x = \frac{1}{4}L_{ch}$  (central channel) and  $x = \frac{1}{2}L_{ch}$  (inlet bend).

precision does not highly impact mean flow data, but rather gives an indication on the modelling capabilities and whether the friction factor is applied accurately. That is to say, if the variations in the pressure drop measurements fall around  $10^4$ , then similar flow features will occur.

## 4.3.2. Temperature distributions

Accurate temperature distributions of the PCHE are important to examine the thermal performance and any stresses that may occur within the system. Fig. 8 shows the temperature distribution for the solid body and both the hot and cold streams. In Fig. 8a, the thermal

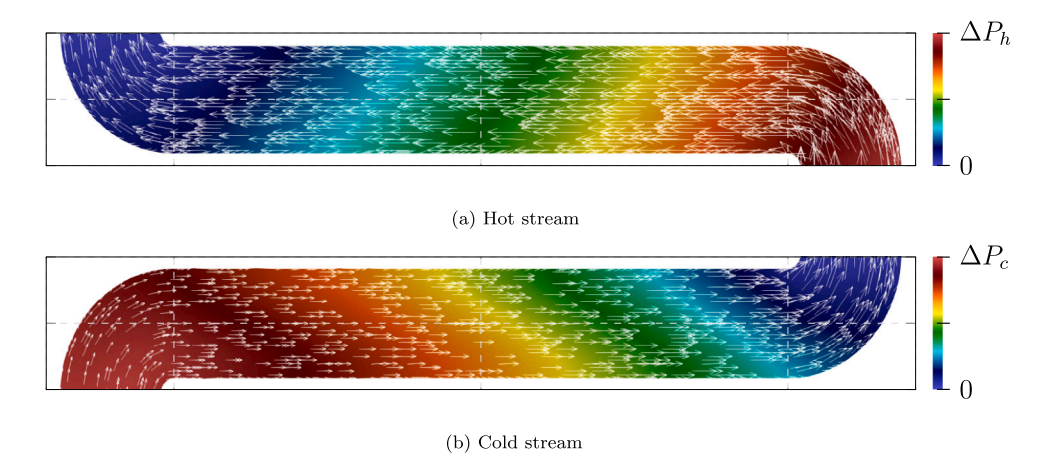


Fig. 7. Contour profiles of mean fluid pressure,  $P_l$  [Pa], with white velocity vectors superimposed. The colour ranges shows the relative pressure drop:  $\Delta P_h = 7839$  [Pa] and  $\Delta P_c = 3199$  [Pa].

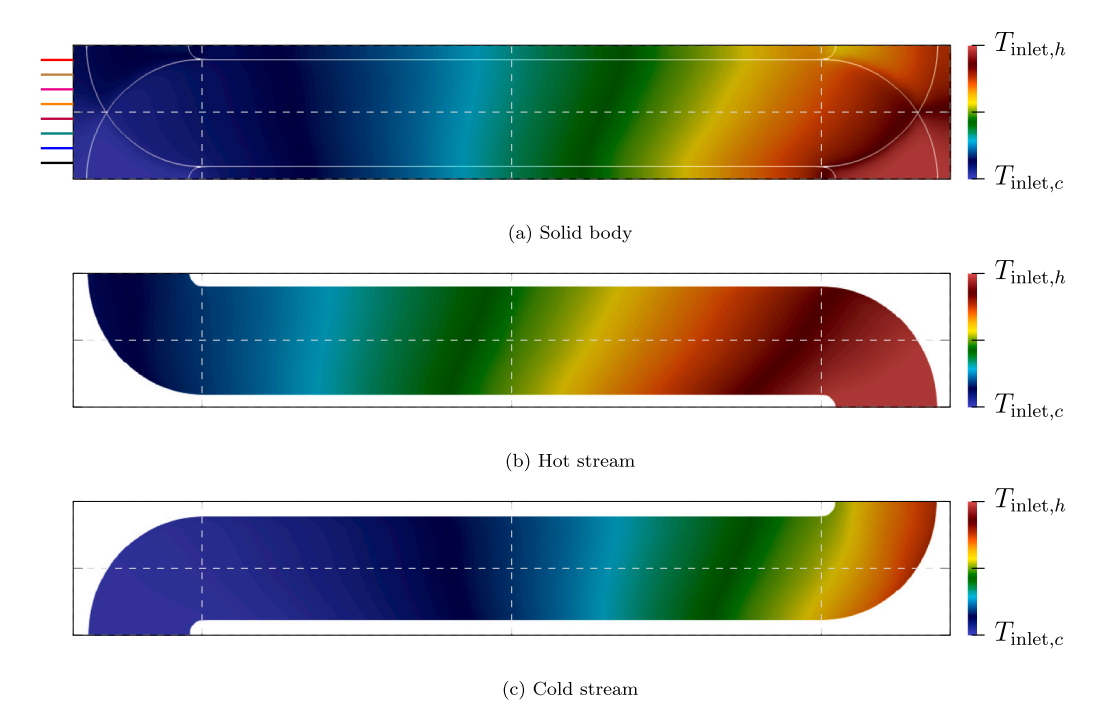


Fig. 8. Contour profiles of the mean temperature distribution, T [K], for the solid body and fluid streams. The colour ranges from  $T_{c,\text{inlet}} = 296.65$  [K] (blue) to  $T_{h,\text{inlet}} = 475.45$  [K] (red). The outline of the fluid streams is superimposed in white on the solid body for improved visuals.

distribution of the solid body from the cold inlet (Region  $(II)_c$ ) to the middle of the central channel (Region  $(I)_c$ ) is dominated by the heat transfer from the cold stream, as a result of the relatively high specific heat capacity of the cold fluid in the temperature region 296.95 [K] <  $T_c$  < 320 [K]. This means that the hot stream fluid cools rapidly in this region with strong heat convection from the cold stream via the solid. The hot inlet (Region  $(II)_h$ ) exhibits a large sharp thermal decrease as the hot fluid turns and goes from a single fluid stream to a multi-fluid stream. The outlet measurements for this case can be seen in Table 4, which are  $T_{h, \text{outlet}} = 318.22$  [K] and  $T_{c, \text{outlet}} = 420.84$  [K]. The data for the hot outlet fall slightly outside the MATLAB numerical results and experimental error bounds, but is captured well for the cold outlet.

To further assess model performance, Fig. 9 displays the solid body temperature distribution along eight experimental instrumentation fibres along the stream direction with equal spacing  $W_{ch}/9$  in the transverse direction (Jentz, 2021). The temperature graphs are staggered by 100 [K] for visual aid, where each colour represents a unique

location, as can be seen in Fig. 8a. Overall, the model matches well with the experimental measurements and Matlab predictions. There is some discrepancy between the experimentally measured values and the model predictions near both ends of the solid body, due to the local cooling action of the protruding capillaries used to house the fibres. These dips in temperature only exist within the fibre sensors and not within the PCHE itself. It should also be noted that the minimum and maximum temperatures recorded from the experimental reading are  $\sim 315~\rm [K]$  and  $\sim 515~\rm [K]$ , which is above and below the hot and cold inlet temperatures, respectively. This means that there is some discrepancy and dependency on the experimental devices, which will be addressed in future work.

Fig. 10 displays the current predictions of the magnitude of the thermal gradient for the solid body,  $|\nabla T_s|$ , and is compared qualitatively with the experimental readings (Jentz, 2021). There are 4 specified regions within the grey dashed circles that display certain thermal dynamics, which are discussed.

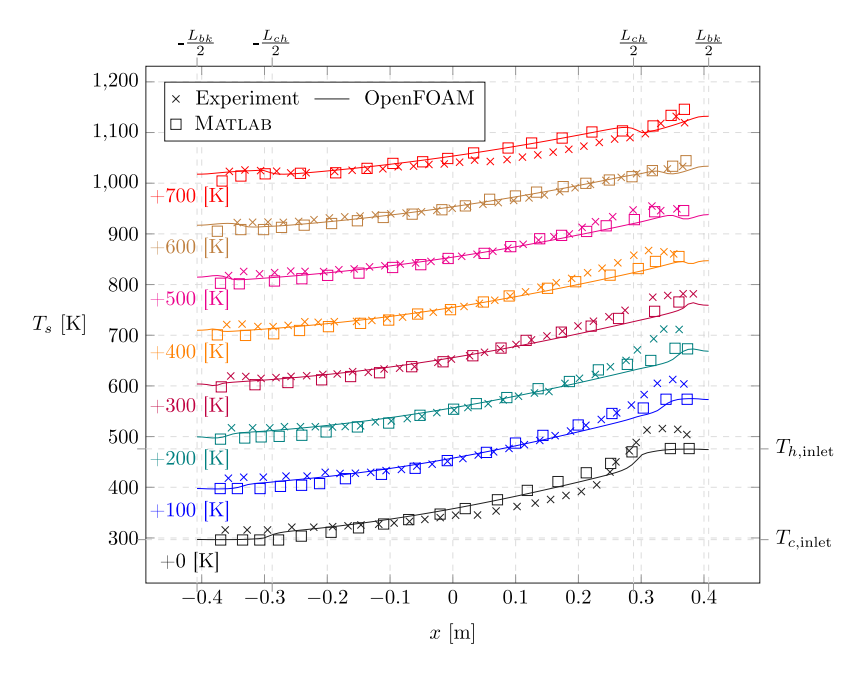


Fig. 9. Comparison of the temperature profile of the solid body,  $T_s$  [K], along the eight experimental instrumentation fibres, Matlab model predictions (Jentz and Anderson, 2020), and current OpenFOAM model predictions. Each colour represents a different equidistant spacing along y with increments  $W_{ch}/9$ .

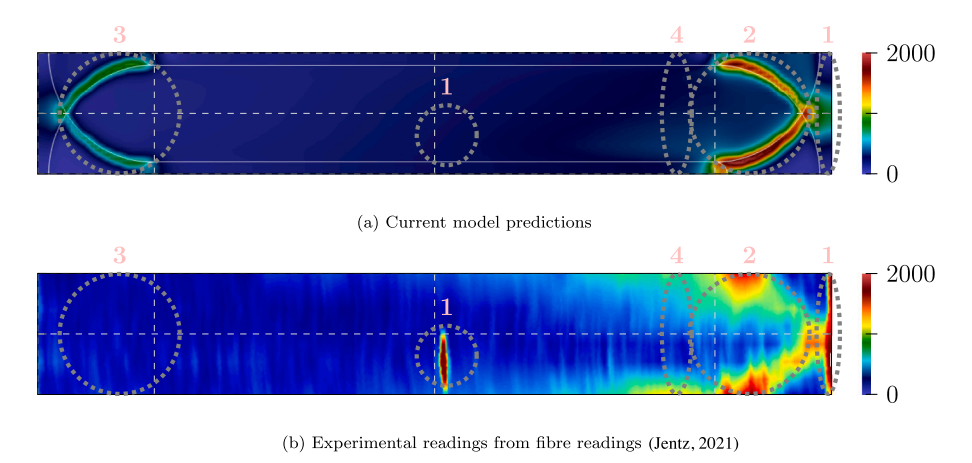


Fig. 10. Comparison of the contour profiles of the temperature gradient magnitude of the solid body,  $|\nabla T_s|$ , for the current model and experimental readings. The colour ranges from  $0 \text{ [K^{-1}]}$  (blue) to 2000  $\text{[K^{-1}]}$  (red).

- The experimental data in these regions are neglected as the local peaks are produced by fibre noise creating some non-physical gradient reading.
- 2. Thermal stress concentrations are highest at the entrance of the hot stream and exit of the cold stream. These occur because there are local cross-flow conditions within the inlet and outlet of the recuperator. The model can predict these peaks well and their distribution, such as the local stress in the inner bend of the hot and cold stream.
- 3. There exists some model prediction of local peaks in this region when the solid body contains a single fluid, similarly to region 2. This could be explained by the role of sensitivity of the thermal properties on the cold stream or by the experimental data readings limitations in low mass flow cases. Both of these points will need to be addressed in future work.
- 4. As the hot stream fluid flows around the bend from the inlet, there is heat loss to the external walls of the solid. The thermal gradients from the solid wall to the centre of the solid also exist within the experimental data, although they are more dispersed in nature and less concentrated in the near-wall region as seen in the current model predictions.

#### 5. Conclusions

The main conclusions of this work are summarised below:

- A finite volume C++ based open-source code is developed within OpenFOAM to predict macro-scale thermal-hydraulic features of compact printed circuit heat exchangers. The chtMultiRegionFoam solver is adapted to incorporate porosity, and a user-friendly coding package is developed to determine quick and reliable results, which is made freely available (https://github.com/MikeMcDermott-Code/PCHE).
- The PCHE is represented as a homogenised volume by considering three uniquely defined regions (hot stream, cold stream, and solid body), which occupy the same volume in regions of fluidsolid overlap. The momentum transport/hydraulic solution is governed by the Navier–Stokes equation with an additional resistance source term accounting for the micro-channels in the form of experimentally measured correlations from frictional drag.
- The linear assumption on cross-flow variations is examined and the hydraulic solution is calculated. Heat transfer between fluid

- stream regions and the solid body is addressed with a volume-volume coupling (cellVolumeWeight interpolation method) through a term of volumetric thermal resistance,  $R_{s\rightarrow l}$ , with the Nusselt number dependent on experimentally determined correlations.
- An example case is presented with an experimental airfoil  $\mathrm{CO}_2\text{-}\mathrm{CO}_2$  PCHE. Thermal distribution predictions are validated against the gathered experimental data from instrumental optical fibres and are also compared with the finite-element MATLAB results within the literature. The model works well to show the general distribution and also the thermal stress characteristics found within the data.
- The modelling strategy can be applied to a range of PCHE designs such as those with multi-stream passages and fluids such as helium and liquid metals. The thermal performance and thermal stress profiles can be adequately predicted in a fast and robust way, and therefore highlight potential design flaws in the safety evaluation of nuclear reactors.
- Further work aims to couple the current macro approach with microscale unit cells for an open-source multiscale modelling package.

#### CRediT authorship contribution statement

**M. McDermott:** Writing – original draft, Visualization, Validation, Software, Methodology, Investigation, Formal analysis, Data curation, Conceptualization. **S. He:** Writing – review & editing, Supervision, Funding acquisition, Conceptualization.

#### Declaration of competing interest

The authors declare that they have no known competing financial interests or personal relationships that could have appeared to influence the work reported in this paper.

#### Data availability

Data will be made available on request.

## Acknowledgements

The research is funded by EPSRC, United Kingdom through grant reference EP/T002395/1. Additional funding was also received from EPSRC, United Kingdom grant EP/T026685/1. The authors would like to thank the University of Wisconsin (Mark Anderson, Nicholas Thoreson, and Ian Jentz), for their support in this project.

#### References

- Aneesh, A.M., Sharma, A., Srivastava, A., Vyas, K.N., Chaudhuri, P., 2016. Thermal-hydraulic characteristics and performance of 3D straight channel based printed circuit heat exchanger. Appl. Therm. Eng. 98, 474–482. http://dx.doi.org/10.1016/j.applthermaleng.2015.12.046.
- Cong, T., Wang, Z., Zhang, R., Wang, B., Zhu, Y., 2021. Thermal-hydraulic performance of a PCHE with sodium and sCO2 as working fluids. Ann. Nucl. Energy 157, 108210. http://dx.doi.org/10.1016/j.anucene.2021.108210.
- Della Torre, A., Montenegro, G., Onorati, A., Khadilkar, S., Icarelli, R., 2019. Multi-scale CFD modeling of plate heat exchangers including offset-strip fins and dimple-type turbulators for automotive applications. Energies 12 (15), 2965. http://dx.doi.org/ 10.3390/en12152965.

- Dmitriev, S., Kurkin, A., Dobrov, A., Doronkov, D., Pronin, A., Solntsev, D., 2023. CFD modeling of heat exchanger with small bent radius coils using porous media model. Fluids 8 (5), 141. http://dx.doi.org/10.3390/fluids8050141.
- El-Hakim, N., Assaf, J., Nehme, B., Zeghondy, B., Said, W., Jelwan, J., 2022. CFD analysis and heat transfer characteristics of printed circuit heat exchanger. J. Therm. Eng. 8 (3), 335–348. http://dx.doi.org/10.18186/thermal.1117345.
- Feichtner, A., Mackay, E., Tabor, G., Thies, P.R., Johanning, L., Ning, D., 2021. Using a porous-media approach for CFD modelling of wave interaction with thin perforated structures. J. Ocean Eng. Mar. Energy 7 (1), 1–23. http://dx.doi.org/10.1007/s40722-020-00183-7.
- Greiciunas, E., Borman, D., Summers, J., Smith, S.J., 2019. A multi-scale conjugate heat transfer modelling approach for corrugated heat exchangers. Int. J. Heat Mass Transfer 139, 928–937. http://dx.doi.org/10.1016/j.ijheatmasstransfer.2019. 05.086.
- He, S., Wang, M., Tian, W., Qiu, S., Su, G.H., 2022. Development of an OpenFOAM solver for numerical simulations of shell-and-tube heat exchangers based on porous media model. Appl. Therm. Eng. 210, 118389. http://dx.doi.org/10.1016/j.applthermaleng.2022.118389.
- Higuera, P., Lara, J.L., Losada, I.J., 2014. Three-dimensional interaction of waves and porous coastal structures using OpenFOAM®. part I: Formulation and validation. Coast. Eng. 83, 243–258. http://dx.doi.org/10.1016/j.coastaleng.2013.08.010.
- Jentz, I.W., 2021. Thermohydraulic and Mechanical Modeling of Printed Circuit Heat Exchangers for Next Generation Nuclear Service (Ph.D. thesis). The University of Wisconsin - Madison. United States - Wisconsin.
- Jentz, I.W., Anderson, M.H., 2020. Coupled heat transfer and hydraulic modeling of an experimental printed circuit heat exchanger using finite element methods. J. Therm. Sci. Eng. Appl. 13 (031017), http://dx.doi.org/10.1115/1.4048312.
- Kim, I.H., No, H.C., 2012. Physical model development and optimal design of PCHE for intermediate heat exchangers in HTGRs. Nucl. Eng. Des. 243, 243–250. http: //dx.doi.org/10.1016/j.nucengdes.2011.11.020.
- Li, X., Su, X., Gu, L., Zhang, L., Sheng, X., 2022. Numerical study of low pr flow in a bare 19-rod bundle based on an advanced turbulent heat transfer model. Front. Energy Res. 10, http://dx.doi.org/10.3389/fenrg.2022.922169.
- Liu, G., Huang, Y., Wang, J., Liu, R., 2020. A review on the thermal-hydraulic performance and optimization of printed circuit heat exchangers for supercritical CO2 in advanced nuclear power systems. Renew. Sustain. Energy Rev. 133, 110290. http://dx.doi.org/10.1016/j.rser.2020.110290.
- Locatelli, G., Mancini, M., Todeschini, N., 2013. Generation IV nuclear reactors: Current status and future prospects. Energy Policy 61, 1503–1520. http://dx.doi.org/10. 1016/j.enpol.2013.06.101.
- Maes, J., Menke, H.P., 2022. GeoChemFoam: Direct modelling of flow and heat transfer in micro-CT images of porous media. Heat Mass Transf. 58 (11), 1937–1947. http://dx.doi.org/10.1007/s00231-022-03221-2.
- Nestell, J., Sham, S., 2015. ASME Code Considerations for the Compact Heat Exchanger. Tech. Rep. ORNL/TM-2015/401, Oak Ridge National Lab. (ORNL), Oak Ridge, TN (United States), http://dx.doi.org/10.2172/1214514.
- Saeed, M., Berrouk, A.S., Wahedi, Y.F.A., Singh, M.P., Dagga, I.A., Afgan, I., 2022. Performance enhancement of a C-shaped printed circuit heat exchanger in supercritical CO2 brayton cycle: A machine learning-based optimization study. Case Stud. Therm. Eng. 38, 102276. http://dx.doi.org/10.1016/j.csite.2022.102276.
- Su, X.-K., Li, X.-W., Wang, X.-Y., Chen, Q.-J., Shi, Q.-W., Qiu, J., Gu, L., 2023. Coupling heat transfer study of liquid sodium and supercritical carbon dioxide in a PCHE straight channel based on a four-equation model. Ann. Nucl. Energy 192, 109976. http://dx.doi.org/10.1016/j.anucene.2023.109976.
- Urquiza, E., Lee, K., Peterson, P.F., Greif, R., 2013. Multiscale transient thermal, hydraulic, and mechanical analysis methodology of a printed circuit heat exchanger using an effective porous media approach. J. Therm. Sci. Eng. Appl. 5 (041011), http://dx.doi.org/10.1115/1.4024712.
- Whitaker, S., 1996. The Forchheimer equation: A theoretical development. Transp. Porous Media 25 (1), 27–61. http://dx.doi.org/10.1007/BF00141261.
- Xiuqing, L., Le Pierres, R., Dewson, S.J., 2006. Heat Exchangers for the Next Generation of Nuclear Reactors. American Nuclear Society ANS, United States.
- Zhu, Q., Pishahang, M., Caccia, M., Kelsall, C.C., LaPotin, A., Sandhage, K.H., Henry, A., 2022. Validation of the porous medium approximation for hydrodynamics analysis in compact heat exchangers. J. Fluids Eng. 144 (081403), http://dx.doi.org/10. 1115/1.4053898.
- Żuk, P.J., Tużnik, B., Rymarz, T., Kwiatkowski, K., Dudyński, M., Galeazzo, F.C.C., Krieger Filho, G.C., 2022. OpenFOAM solver for thermal and chemical conversion in porous media. Comput. Phys. Comm. 278, 108407. http://dx.doi.org/10.1016/ j.cpc.2022.108407.